Electric Field Simulation of Permittivity and Conductivity Graded Materials (ε/σ-FGM) for HVDC GIS Spacers

Rachmawati, Hiroki Kojima and **Naoki Hayakawa**
Department of Electrical Engineering, Nagoya University
Furo-cho, Chikusa-ku, Nagoya 464-8603, Japan

Katsumi Kato
Department of Electrical Engineering and Information Science
National Institute of Technology, Niihama College
7-1 Yaguma-cho, Niihama, Ehime 792-8580, Japan

Nabila Zebouchi
Cardiff University
Cardiff CF24 3AA, UK

ABSTRACT

This paper discusses the application of the novel technology - functionally graded material (FGM) which combines both spatial permittivity (ε) and conductivity (σ) distributions with the aim to control the electric field around DC-GIS spacer. Some distribution types of ε and/or σ in the spacer bulk, such as U-type and graded to higher conductivity (GHC) are investigated through electric field simulation, in comparison to the uniform spacer with constant ε and σ distributions. The electric field relaxation effect of each distribution type of ε/σ-FGM under DC steady state, DC polarity reversal, DC-on, and lightning impulse voltage superimposed on DC steady state condition are obtained. The results show that ε/σ-FGM with U-type permittivity and GHC-type conductivity distribution of which low σ is applied near the high voltage side of the DC-GIS spacer is the most effective in reducing the maximum electric field under all stated conditions.

Index Terms — **functionally graded materials (FGM), electric field grading, DC steady state, polarity reversal, conductivity, permittivity**

1 INTRODUCTION

THE requirement of a larger scale of power transmission over long distances has encouraged the development of high voltage direct current (HVDC) system which offers high power transmission efficiency with low transmission losses. As power generation from renewable energy also expands in recent years, HVDC system beneficially serves for purposes such grid interconnections and frequency conversions. Besides, the compact structure of DC power apparatus is advantageous in terms of space, cost, and particularly SF_6 gas reduction [1-2].

On the other hand, unlike AC, designing an insulation system for DC power apparatus has its own complications, since more parameters other than material aging, such as thermo-electrical interdependencies need to be considered [3]. Specifically, the solid insulation of GIS or GIL, such as the spacer becomes the critical component that usually leads to insulation failure. Immediately after the DC voltage is applied, capacitive fields take place around the spacer which transit to resistive fields over time under DC steady state. The field transition is influenced by both the permittivity and the conductivity of the material, where the conductivity in turn is affected by the temperature gradient and the electric field distribution within the insulation system. These factors can lead to local electric field enhancement, that if uncontrolled may cause insulation breakdown [3-5].

For that reason, controlling the electric field distribution around GIS spacer under DC operating conditions is indispensable. Many attempts in reducing the electric field stress have been taken, such as applying shielding electrodes and radii ratios optimization which complicate the design, yet limits the performance improvement. Electric field grading concepts through geometry (bulk) and potential (surface) are reviewed for this problem [6].

In our past works, a scale model of functionally graded materials (FGM) with graded permittivity has been proposed and applied to AC-GIS spacer. The simulation result shows that

Manuscript received on xx Month 20yy, in final form xx Month 20yy, accepted xx Month 20yy. Corresponding author: Rachmawati.

the maximum electric field strength in SF_6 gas can be reduced by 64% compared to a spacer with uniform permittivity. Additionally, the discharge inception voltage can be improved by 70% at 0.4 MPa [7-8].

Similar research on ε-FGM was also conducted by other groups who proposed permittivity modification on various types of spacer through numerical topology optimization. The method results in improved electric field distribution and reduced the maximum electric field more than 50%. In addition, an ε-FGM fabrication concept through 3D printing technology was introduced. However, this approach is still considered as expensive and requires modification for FGM implementation [9]. Another paper has reported about charge transport mechanism and surface charge control methods on novel HVDC spacers in which one of them is through surface conductivity modification [10].

Therefore, for DC application, an FGM with graded permittivity and/or conductivity applied to the spacer bulk is required to fulfill the purpose of electric field grading, under steady-state DC stress and time-varying stress that occurs during DC-on, polarity reversal, or superimposed lightning impulse voltage on DC steady state [11-12]. In this paper, two different types of FGM with graded permittivity (ε) and/or conductivity (σ) distribution, which are the U-type and graded-to-higher conductivity (GHC)-type, are discussed for electric field grading under different DC stresses. The electric field simulation is performed to verify the electric field relaxation effect around ε/σ-FGM spacer in comparison to the spacer with uniform (constant) ε and σ.

2 CONCEPT OF DC-FGM AND SIMULATION MODEL

2.1 CONCEPT OF DC-FGM

The basic concept of electric field grading by FGM can be explained by the electric field distributions in a GIS which consist of capacitive and resistive electric fields. Derived from Ampere's Law of Maxwell's equation, the total current density is shown by equation (1),

$$\vec{J} = \vec{J_c} + \vec{J_d} = \sigma\vec{E}\varepsilon\frac{\partial\vec{E}}{\partial t} \quad (1)$$

where $\vec{J_c}$ is the conduction current by moving charges, $\vec{J_d}$ is the displacement current resulted from the time-dependent electric field, σ and ε are the electric conductivity and the permittivity of the material to which the electric field $\vec{E}$ is applied. By applying vector identity and Fourier transform, the continuity equation is obtained and can be simply written as equation (2),

$$\nabla\cdot\left(\varepsilon - j\frac{\sigma}{2\pi f}\right)\nabla\varphi = 0 \quad (2)$$

where f is assumed to be the frequency of the applied AC voltage, and φ is the potential.

Depending on the applied voltage, for AC (capacitive) fields, the displacement current with decisive ε is usually dominant. On the other hand, for DC (resistive) fields that occur in DC steady state condition, only the conduction current with σ of the material is needed to be considered.

Nevertheless, both AC and DC fields take place under the applied voltage pattern in DC application, as illustrated in Figure 1. Mixed electric fields can occur during DC polarity reversal, turn off, and other conditions which possibly happen during operation, such as the superimposed lightning impulse (LI) voltage on DC steady state. Considering these phenomena, in order to control the electric field distributions in the insulation system of a HVDC GIS, the FGM application to the spacer should incorporate both ε and σ grading, which is called as ε/σ-FGM. An example of this scheme is also illustrated in Figure 2. In this work, ε and σ distributions in the spacer bulk are assumed to be independent of each other.

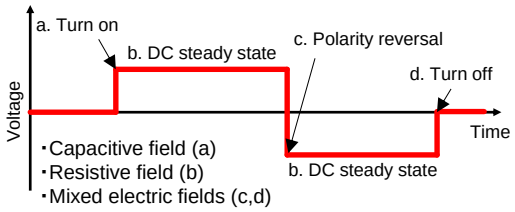

Figure 1. Voltage pattern in HVDC power apparatus.

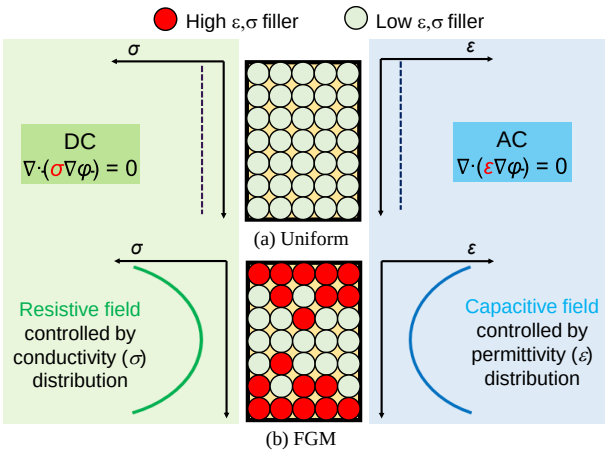

Figure 2. Electric field control by permittivity and conductivity distributions of the insulating material.

2.2 PERMITTIVITY/CONDUCTIVITY DISTRIBUTION OF ε/σ–FGM AND SIMULATION CONDITIONS

The main idea of grading the material properties throughout the spacer's material is to differentiate the spacer parts that get higher stress than the others with higher σ, so that E around those parts can be relaxed. Therefore, smooth grading of σ and/or ε is required to develop more uniformly distributed E stress within the spacer bulk and along the spacer length.

There are two types of σ grading and one type of ε grading which are simulated in the current works. Together with the simulation model of 320 kV DC GIS cone-type spacer [13-14], the shape and range of graded ε/σ-FGM in comparison with uniform spacer is shown in Figure 3. These graded ε and σ are applied to the FGM spacer longitudinally along z axis by controlling the density of the filler with high ε and σ through flexible mixture casting (FMC) method [8]. This method allows the composite mixture to be accumulated in a spacer mold from z = 0 up to z = 280 mm, so that the ε and σ values change gradually in z direction as shown in Figure 3.

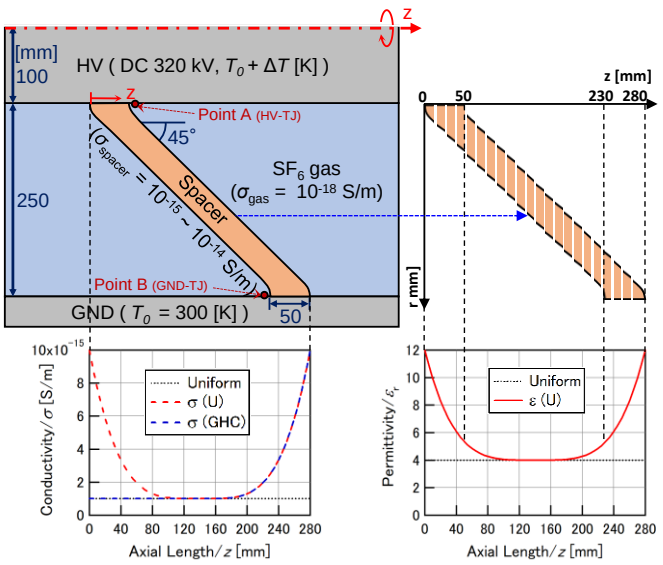

Figure 3. DC FGM cone-type spacer simulation model with conductivity and permittivity distribution types.

The conductivity distribution σ(U) with U-type σ grading has the highest σ (10^{-14} S/m) at the spacer interface with the high voltage (HV) side as well as at the spacer interface with the ground (GND) side. The high σ from both ends is graded toward the lowest σ (10^{-15} S/m) at the middle part of the spacer. This type of grading is expected to be able to reduce high E in the vicinity of the concave surface of the spacer near the HV side (the triple junction of HV side/ HV-TJ) and in the vicinity of the convex surface of the spacer near the GND side (GND-TJ). Hence, E is more uniformly distributed in the middle part of the spacer with lower σ.

The conductivity distribution σ(GHC) with grading-to-higher-conductivity is considered for E relaxation at DC polarity reversal (DC-PR). According to [15], the electric field at DC-PR (E_{PR}) can be calculated by equation (3),

$$E_{PR} = |2E_{AC} - E_{+DC}| \tag{3}$$

where E_{AC} and E_{DC} are the capacitive and resistive field, respectively. The spacer with σ(U) having higher σ near HV-TJ will cause E_{DC} component at HV-TJ reduced, hence the E_{PR} increases. For this purpose, σ(GHC) is more likely to lead to better results, as it has low σ around HV-TJ up to the middle part of the spacer, resulting in enhanced E_{DC} component around that area. Thus, E_{PR} is reduced.

Additionally, due to E_{AC} occurrence under DC-PR or other conditions with superimposed voltages, ε grading in U-type where the spacer parts at the interface with HV and GND sides have high ε (ε_r = 12) and the middle part of the spacer has low ε (ε_r = 4) is expected to reduce high E around HV electrode/spacer and GND electrode/spacer interfaces [7].

E simulation is conducted using Comsol Multiphysics® by finite element method. Some combinations of ε and σ distributions are applied to the cone-type spacer model in Figure 3 under four voltage conditions given in Table 1. Based on the E simulation results under DC steady state and polarity reversal, the most effective FGM spacer model to the electric field grading is selected and compared with the uniform spacer under DC-on and superimposed LI on DC steady state.

Table 1. Electric field simulation conditions.

Applied Voltage	Uniform	FGM	
	ε/σ distribution	σ distribution	ε distribution
DC steady state	Constant (ε_r = 4, σ = 10^{-15} S/m	constant	U-type
		U-type	constant
		U-type	U-type
		GHC	U-type
Polarity reversal		constant	U-type
		U-type	constant
		U-type	U-type
		GHC	U-type
DC-on		GHC	U-type
Superimposed LI on DC steady state		GHC	U-type

In the simulation, σ depends on the temperature (T) and the electric field strength (E) as described in equation (4) [2-3, 16],

$$\sigma(T,E) = \sigma_0 \exp\left(-\frac{W}{kT}\right)\exp(aE) \tag{4}$$

where σ_0 is the specific conductivity constant in S/m, W = 0.95 eV is the thermal activation energy, k is Boltzmann constant in eV/K, and a = 0.08 mm/kV is the electric field dependency coefficient. The temperature effect is examined by changing the temperature of the high voltage conductor as $T_0 + \Delta T$ with ΔT ranging from 0 to 70 K, while keeping the temperature of the ground tank at T_0 = 300 K. This temperature distribution is calculated by the heat conduction analysis based on equation (5),

$$\nabla \cdot (\kappa \nabla T) = 0 \tag{5}$$

where κ is the thermal conductivity.

3 ELECTRIC FIELD SIMULATION RESULTS OF ε/σ-FGM SPACERS

3.1 DC STEADY STATE

In DC steady state simulation, 320 kV DC voltage is applied to the HV conductor. Then, the maximum electric field strength (E_{max}) in gas around the uniform and each type of FGM spacers is calculated with ΔT from 0 to 70 K, as shown in Figure 4.

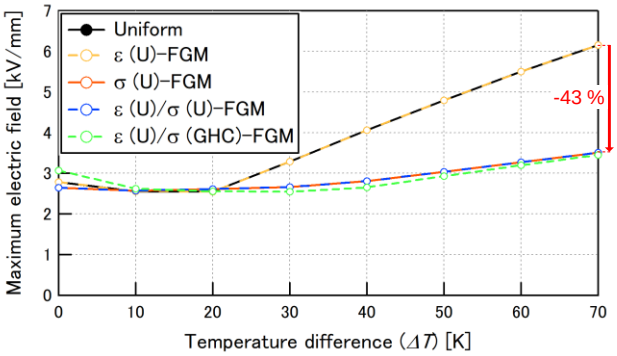

Figure 4. Maximum electric field strength in gas around the spacer under DC steady state.

The graph shows that E_{max} around the uniform spacer at each ΔT is the same as that around ε(U)-FGM spacer. Similarly, E_{max} around σ(U)-FGM spacer is the same as that around ε(U)/σ(U)-FGM spacer. This result proves that under DC steady state condition, whether it is graded or not, ε of the spacer does not contribute to E distribution in the insulation system, because ε

is not decisive under DC steady state. Only the FGM spacers with graded σ can suppress E_{max} despite the increase in ΔT. E_{max} reduction of σ(U)-FGM and ε(U)/σ(GHC)-FGM spacers reaches 43% at ΔT = 70 K.

However, at ΔT < 10 K, E_{max} around ε(U)/σ(GHC)-FGM spacer is higher than those of the uniform spacer and σ(U)-FGM spacer. This is because at lower ΔT at which the E_{max} location is within the HV-TJ, the σ distribution ε(U)/σ(GHC)-FGM spacer near the HV side is at the same level as that of the uniform spacer (low σ), hence E in the vicinity of HV-TJ is enhanced compared to σ(U)-FGM spacer that has higher σ in that part. This can be seen in Figure 5 which shows E distribution around the spacer models at ΔT of 0 K, 30 K, and 60 K along with the spots of E_{max}.

Besides, unlike the uniform spacer, since the ε(U)/σ(GHC)-FGM spacer has higher σ at the end part near the ground side, the equipotential lines are pushed from the ground side toward the middle and the part near HV side that has lower σ. Hence, at lower ΔT, E of ε(U)/σ(GHC)-FGM spacer is even higher than that of the uniform spacer.

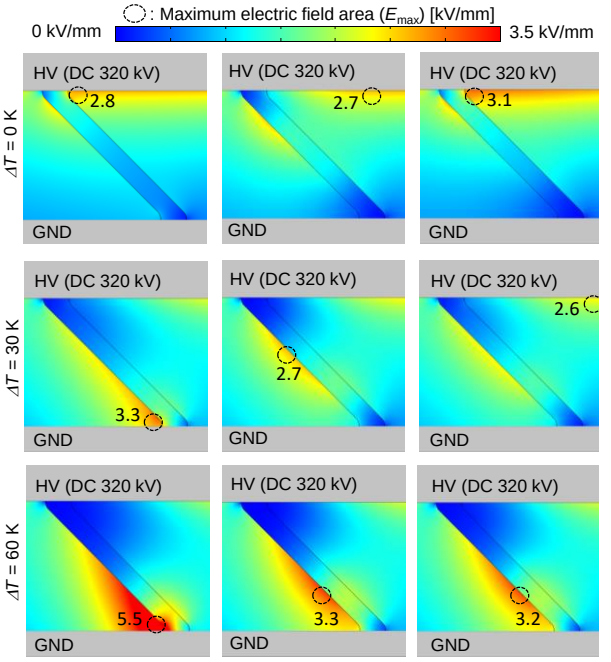

(a) Uniform (b) σ(U)-FGM (c) ε(U)/σ(GHC)-FGM

Figure 5. E distribution around spacers under DC steady state.

3.2 DC POLARITY REVERSAL

At DC-PR, there is a sudden change in the voltage magnitude from positive 320 kV to negative 320 kV over a short switching time. Therefore, both ε and σ are decisive on E distribution. According to equation (3), E_{DC}, E_{AC}, and E_{PR} around uniform and various FGM spacers at ΔT = 20 K are presented in Figures 6, 7, and 8, respectively.

Figures 6a and 6b show that E distribution around the uniform spacer is similar to that of ε(U)-FGM spacer, which proves that ε grading without σ grading in an FGM spacer does not affect E distribution under DC steady state condition. On the other hand, Figures 6c, 6d, and 6e show that E distribution around FGM spacers with graded σ, regardless of the ε grading, is different

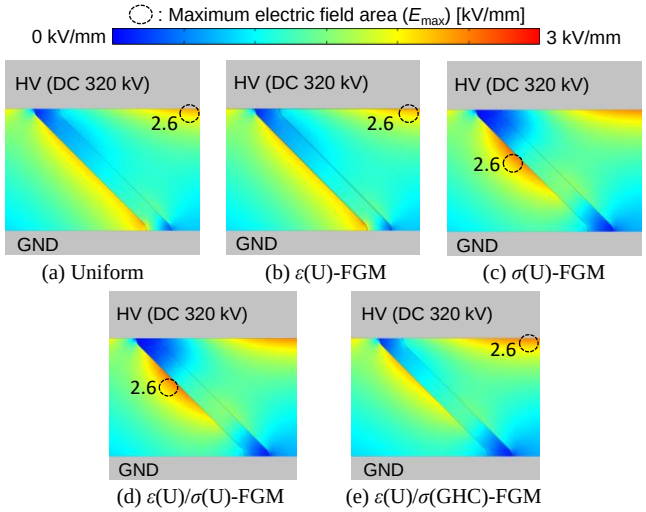

(a) Uniform (b) ε(U)-FGM (c) σ(U)-FGM

(d) ε(U)/σ(U)-FGM (e) ε(U)/σ(GHC)-FGM

Figure 6. E distribution under DC steady state (E_{+DC}) at ΔT = 20 K.

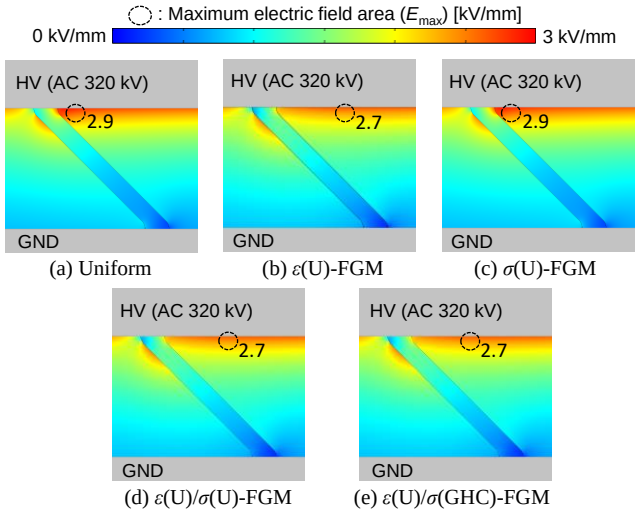

(a) Uniform (b) ε(U)-FGM (c) σ(U)-FGM

(d) ε(U)/σ(U)-FGM (e) ε(U)/σ(GHC)-FGM

Figure 7. E distribution under AC steady state (E_{AC}) at ΔT = 20 K.

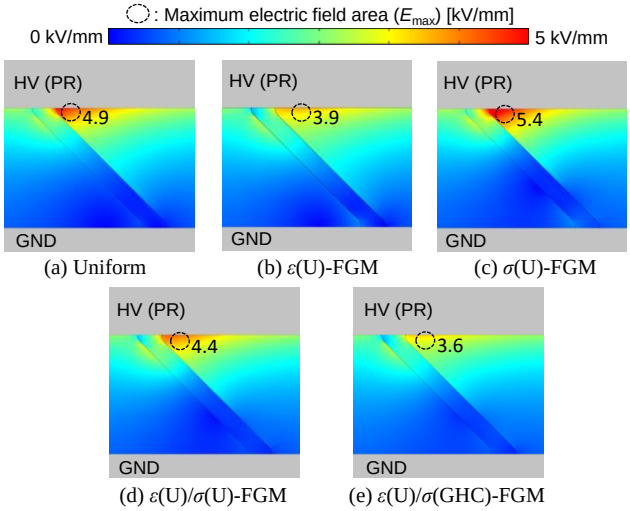

(a) Uniform (b) ε(U)-FGM (c) σ(U)-FGM

(d) ε(U)/σ(U)-FGM (e) ε(U)/σ(GHC)-FGM

Figure 8. E distribution under DC-PR (E_{PR}) at ΔT = 20 K.

from that around uniform spacer. The high E within the HV-TJ and GND-TJ are clearly reduced due to the higher σ of the spacer parts near those locations.

The opposite phenomena can be seen in Figure 7 which illustrates the capacitive field (E_{AC}) distribution. The FGM spacers with graded ε (Figures 7b, 7d, and 7e) have high E_{AC} around HV-TJ, which is reduced owing to the higher ε of the spacer at the spacer/HV conductor interface.

Those E_{DC} and E_{AC} distributions around each spacer determine the E distribution at DC-PR (E_{PR}) as shown in Figure 8, where E_{max} is found around the HV-TJ. The σ(U)-FGM spacer, which is effective in reducing E_{max} under DC steady state, shows on the contrary higher E compared to the uniform spacer at DC-PR (Figure 8c). This is because the E_{AC} around uniform and σ(U)-FGM spacers remain the same (Figures 7a and 7c) and the E_{DC} of σ(U)-FGM spacer at that point is greatly reduced (Figure 6c). As a result, E_{PR} of σ(U)-FGM spacer is higher than that of uniform spacer.

Meanwhile, the FGM spacers with graded ε (Figures 8b, 8d, and 8e) have suppressed E_{PR} compared to uniform spacer. Referring to equation (3), the effect of E_{AC} is more dominant than E_{DC} under PR condition. Therefore, ε grading can reduce E_{AC} component, hence E_{PR} is also lower than that of uniform or σ(U)-FGM spacer.

Particularly, ε(U)/σ(GHC)-FGM spacer results in the lowest maximum electric field strength at polarity reversal (E_{PR}^{max}) among all other ε/σ-FGM spacers. This is due to the fact that the higher σ in the spacer part near the ground side causes potential burden from the ground side shifted toward the middle and upper part of the spacer (near HV side) and slightly increases E_{DC} around those parts with lower σ. Therefore, the resulted E_{PR} near the HV-TJ of ε(U)/σ(GHC)-FGM spacer is also reduced a little bit more compared to ε(U)-FGM or ε(U)/σ(U)-FGM spacers.

In order to compare the effect of each FGM spacer, Figure 9 shows E_{PR}^{max} against ΔT between HV and GND conductors. It can be concluded that at DC-PR, the largest reduction of E_{PR}^{max} at each ΔT is given by ε(U)/σ(GHC)-FGM spacer. The maximum E_{PR} reduction of ε(U)/σ(GHC)-FGM spacer is achieved by 30% at ΔT=10 K compared to uniform spacer. Based on this result, for the next two simulation conditions (DC-on and superimposed lightning impulse on DC steady state), only the E analysis around ε(U)/σ(GHC)-FGM spacer with comparison to uniform spacer will be evaluated.

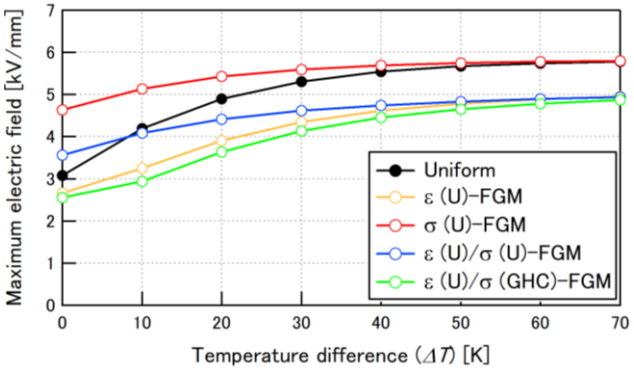

Figure 9. E_{max} under DC-PR (E_{PR}^{max}) against temperature difference ΔT.

3.3 DC-ON

The E analysis under DC-on condition is performed through time dependent simulation where positive 320 kV DC voltage is applied to the HV conductor within 0.01 s switching time. The E characteristics are then evaluated over time until it reaches DC steady state, particularly at points A and B which are the critical points located at HV-TJ and GND-TJ, as illustrated in Figure 3.

Figures 10 and 11 show the E distribution around (a) uniform and (b) ε(U)/σ(GHC)-FGM spacers at different times for ΔT = 20 K and 70 K, respectively.

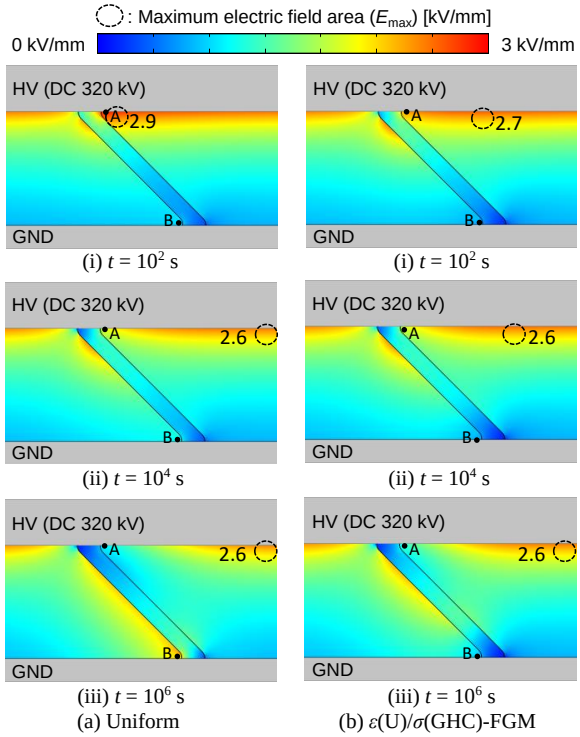

Figure 10. E distribution around (a) uniform spacer and (b) ε(U)/σ(GHC)-FGM spacer during DC-on at ΔT = 20 K.

At lower ΔT (ΔT=20 K), the high E at early stage of the temporal transition (t = 10^2 s) since the voltage is applied, is concentrated near the HV-TJ (point A) and along the HV conductor surface for both spacers. As time passes, for the uniform spacer, the high E is shifted toward point B at t = 10^6 s where the DC steady state has been already reached. However, for ε(U)/σ(GHC)-FGM spacer, the high E distribution is concentrated on the middle part of the spacer at that time, so point B during DC steady state remains clear of high E.

The same situation also applies at higher ΔT (ΔT=70 K), as shown in Figure 11. The high temperature enhances the σ of both spacers near the warm HV side, pushing the potential burden from the HV side toward the GND side. However, the higher σ of ε(U)/σ(GHC)-FGM spacer near the GND side is further enhanced with the temperature rise, causing the high E around point B reduced.

The magnitude of E at both points A and B are more clearly distinguished in Figure 12. At ΔT=20 K (Figure 12a), as soon as DC voltage is applied, E of ε(U)/σ(GHC)-FGM spacer at point A is already lower than that of uniform spacer. This E reduction is caused by graded ε that has effect on E_{AC}. As time passes, the E at point A decreases until it reaches the steady state.

On the contrary, the E at point B around the uniform spacer increases over time due to the displacement of field

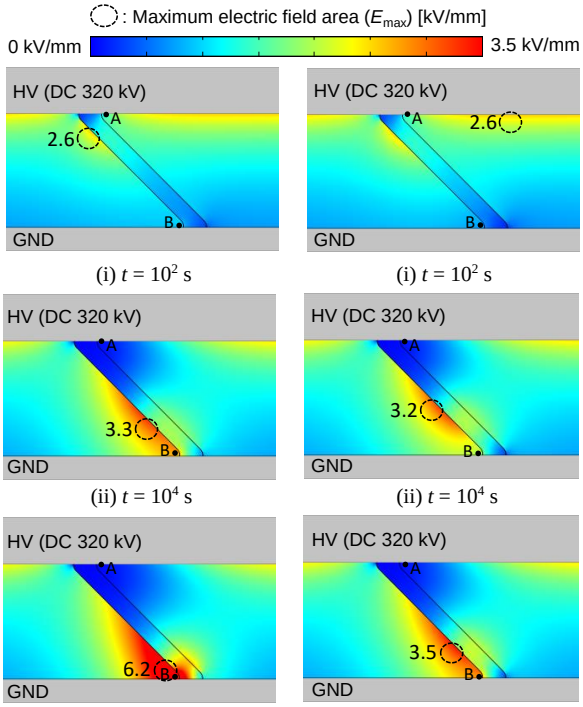

Figure 11. E distribution around (a) uniform spacer and (b) ε(U)/σ(GHC)-FGM spacer during DC-on at ΔT = 70 K.

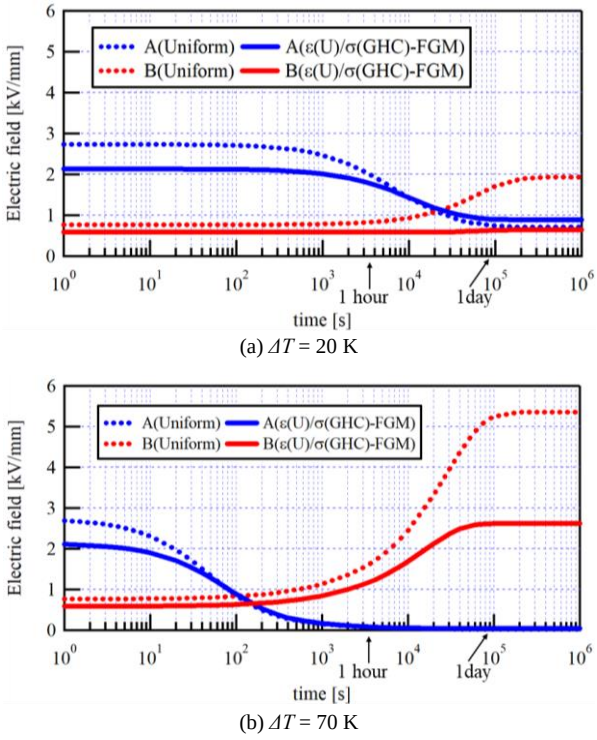

(a) ΔT = 20 K

(b) ΔT = 70 K

Figure 12. Time-varying E distribution at point A near HV-TJ and at point B near GND-TJ of uniform spacer and ε(U)/σ(GHC)-FGM spacer at (a) ΔT = 20 K and (b) ΔT = 70 K.

concentrations from the HV to the GND side. Nevertheless, the E at point B around ε(U)/σ(GHC)-FGM spacer remains the same right from the beginning owing to the higher σ of the spacer near point B.

At ΔT=70 K (Figure 12b), the time-varying electric field at points A and B evolves the same way as that at ΔT=20 K, with higher increase of E at point B as the temperature increases. The transition time required for E_{AC} to shift into E_{DC} during DC-on can also be distinguished from the figures. As ΔT increases, this capacitive-resistive transition time of ε(U)/σ(GHC)-FGM spacer gets shorter.

Figure 13 shows the time-varying E_{max} in gas around (a) uniform spacer and (b) ε(U)/σ(GHC)-FGM spacer for different ΔT from 0 K to 70 K. It is understood that both E_{AC} and E_{DC} of ε(U)/σ(GHC)-FGM spacer are relaxed than those of uniform spacer at each ΔT, which is indicated by the E_{max} location transition from point A to B. The E_{max} reduction is by 43% at ΔT= 70 K, which is consistent with that under DC steady state in Section 3.1.

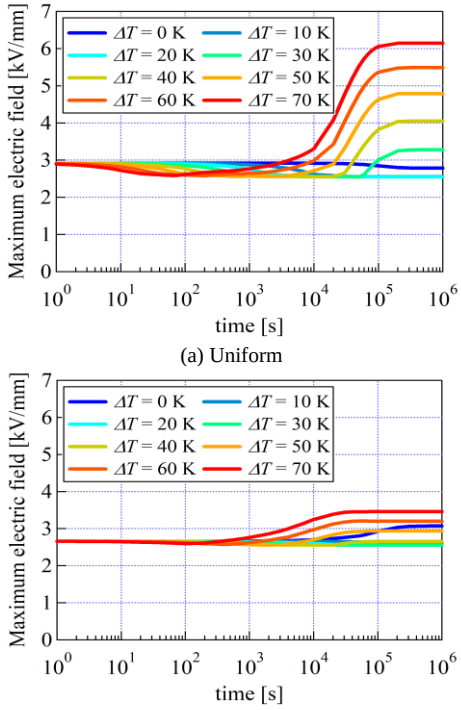

(a) Uniform

(b) ε(U)/σ(GHC)-FGM

Figure 13. Time-varying E_{max} in gas around (a) uniform and (b) ε(U)/σ(GHC)-FGM spacers under different ΔT.

3.4 SUPERIMPOSED LIGHTNING IMPULSE (LI) VOLTAGE ON DC STEADY STATE

The E simulation under superimposed lightning impulse (LI) voltage on DC steady state is performed through time-dependent simulation, i.e. 320 kV DC voltage applied to the HV conductor until DC steady state is reached, then 1175 kV [17] positive and negative LI voltages are superimposed, as illustrated in Figure 14.

Figures 15 and 16 show E distribution around (a) uniform and (b) ε(U)/σ(GHC)-FGM spacers under superimposed standard positive and negative LI of 1175 kV$_{peak}$ on 320 kV DC steady state condition, respectively. According to the figures, under both superimposed positive or negative LI voltage on DC steady state, and with or without ΔT, ε(U)/σ(GHC)-FGM can reduce the E around the HV-TJ and shift the E_{max} location away from the HV-TJ along the HV conductor surface.

In order to obtain the picture quantitatively, Figure 17 indicates the E at point A under different ΔT. Under both

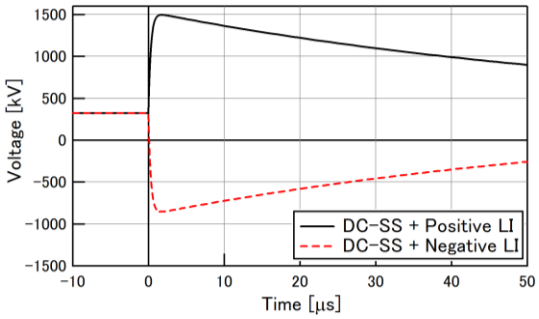

Figure 14. Superimposed LI voltage on DC steady state.

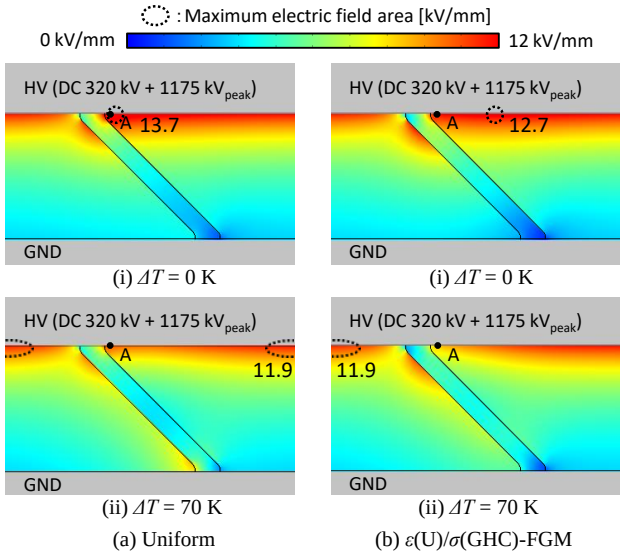

(i) ΔT = 0 K (i) ΔT = 0 K

(ii) ΔT = 70 K (ii) ΔT = 70 K

(a) Uniform (b) ε(U)/σ(GHC)-FGM

Figure 15. E distribution under superimposed positive LI voltage on DC steady state.

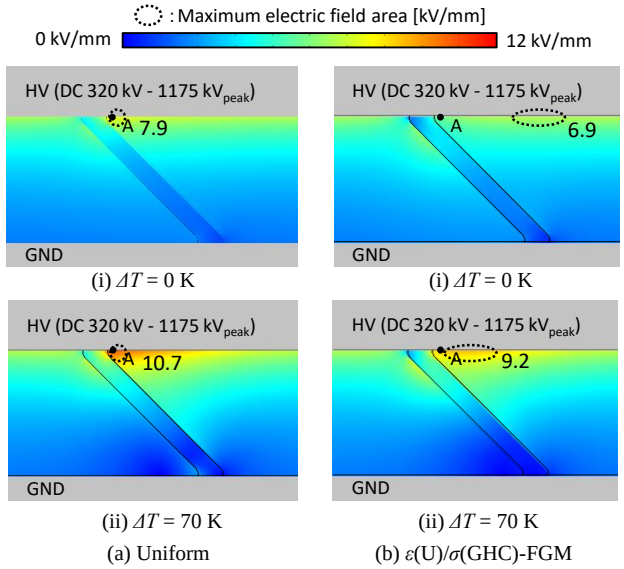

(i) ΔT = 0 K (i) ΔT = 0 K

(ii) ΔT = 70 K (ii) ΔT = 70 K

(a) Uniform (b) ε(U)/σ(GHC)-FGM

Figure 16. E distribution under superimposed negative LI voltage on DC steady state.

superimposed positive and negative LI voltages on DC steady state, the E at point A of ε(U)/σ(GHC)-FGM spacer is constantly lower than that of uniform spacer even with the higher ΔT. The E reduction is 1.6 kV/mm and 2.0 kV/mm under superimposed positive and negative LI, respectively.

Figure 18 shows E_{max} under superimposed positive (E_{+Imp}) and negative (E_{-Imp}) LI voltage on DC steady state against ΔT.

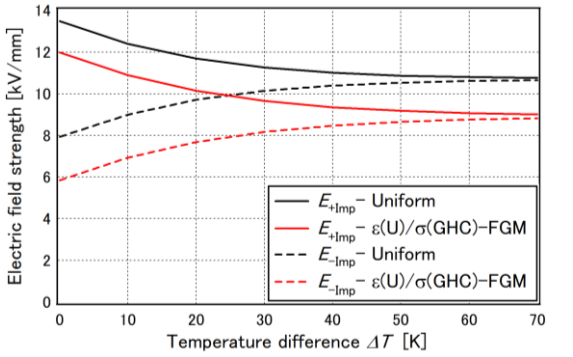

Figure 17. E at point A under superimposed positive and negative LI voltage on DC steady state.

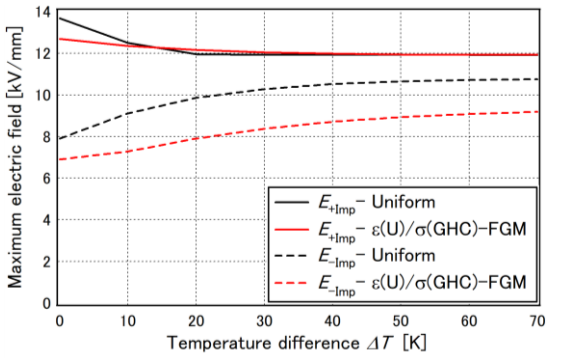

Figure 18. E_{max} under superimposed positive and negative LI voltage on DC steady state.

The maximum reduction of E_{+Imp} around ε(U)/σ(GHC)-FGM spacer is 7% at ΔT= 0 K. The decrease is due to graded ε of ε(U)/σ(GHC)-FGM spacer that reduces E_{AC} around HV-TJ. Meanwhile, the high σ at the GND side of the ε(U)/σ(GHC)-FGM spacer causes potential burden from GND side shifted toward HV side and increases E_{DC} around HV side. Consequently, the E_{+Imp} reduction by this FGM model is relatively small.

When ΔT increases, E_{max} around either uniform or ε(U)/σ(GHC)-FGM spacers converges at approximately 11.9 kV/mm. This value is consistent with the theoretical value of E_{max} at inner conductor of an infinite coaxial cylinder electrodes.

Similar to the case of DC-PR, E_{-Imp} around ε(U)/σ(GHC)-FGM spacer is constantly reduced despite the increase in ΔT. The highest E_{-Imp} reduction by ε(U)/σ(GHC)-FGM application is 20% at ΔT = 10 K.

4 CONCLUSIONS

FGM application with graded ε and σ in a DC GIS spacer has been proposed and the effectiveness in E relaxation has been evaluated under various DC operating conditions. Through E simulation, the following results are revealed.

(1) FGM application with graded σ is effective for E relaxation under DC steady state operation. σ(U)-FGM and ε(U)/σ(GHC)-FGM spacers can reduce the E_{max} by 43% at ΔT of 70 K, compared to uniform spacer.

(2) FGM application with both graded ε and σ is effective to reduce both resistive and capacitive field during other DC operating conditions with rapid voltage change over time, such as polarity reversal, DC-on, and superimposed positive and negative lightning impulse voltage on DC

steady state. The new idea of ε(U)/σ(GHC)-FGM with low σ distribution near HV side of the spacer is currently evaluated as the most effective ε/σ distribution in reducing the E_{max} in gas compared to uniform spacer. It is validated through electric field simulations with E_{max} reduction of 30%, 43%, 7% and 20%, respectively, for each DC operating condition.

For ε/σ-FGM implementation in the future works, currently the actual permittivity and conductivity characteristics of SiC and SiO_2 filled epoxy insulation material have been measured and applied to the electric field analysis in order to gain more actual results with its temperature and electric field dependence properties. As flexible mixture casting (FMC) method has been reported successfully implemented to create ε-FGM spacer with desired ε distribution [8, 18-19], it is expected that with the same arrangement in controlling filler density of the epoxy resin throughout spacer length, the desired permittivity and conductivity distribution can be achieved in fabricating ε/σ-FGM.

ACKNOWLEDGMENT

This work was supported by JSPS KAKENHI Grant Number JP18H01423.

REFERENCES

[1] CIGRE WG B4.44, "HVDC Environmental Planning Guidelines," CIGRE Technical Brochure no. 508, 2012.
[2] M. Hering *et al*, "Investigation of the temperature influence on the breakdown voltage in gas insulated systems under DC voltage stress," *18th Int. Symp. High Voltage Engineering (ISH)*, 2013, OE7-02, pp.1354-1359.
[3] B. Lutz, K. Juhre, and D. Imamovic, "Long-term performance of solid insulators in gas insulated systems under HVDC stress," *19th Int. Symp. High Voltage Engineering (ISH)*, 2015, OD7-4.
[4] M. Hering *et al*, "Requirements on solid insulating materials and gas solid interfaces in compact HVDC gas-insulated systems," *20th Int. Symp. High Voltage Engineering (ISH)*, 2017, OG1-3.
[5] M. Tenzer *et al*, "Compact gas-solid insulating systems for high-field-stress in HVDC applications," *CIGRE SC B3/D1 Colloq.*, 2013, no. 227.
[6] CIGRE WG D1.56, "Field grading in electrical insulation systems," CIGRE Technical Brochure no. 794, 2020.
[7] N. Hayakawa *et al*, "Fabrication and simulation of permittivity graded materials for electric field grading of gas insulated power apparatus," IEEE Trans. Dielectr. Electr. Insul., vol. 23, no. 1, pp. 547-554, Feb. 2016.
[8] N. Hayakawa *et al*, "Simulation on discharge inception voltage improvement of GIS spacer with permittivity graded materials (ε-FGM) using flexible mixture casting method," IEEE Trans. Dielectr. Electr. Insul., vol. 25, no. 4, pp. 1318-1323, Aug. 2018.
[9] W. Li *et al*, "Numerical optimization and 3D-Printing fabrication concept of high voltage FGM insulator," *IEEE PES Asia-Pacific Power and Energy Engineering Conf. (APPEEC)*, 2015.
[10] C. Li *et al*, "Novel HVDC spacers by adaptively controlling surface charges – Part 1: charge transport and control strategy," IEEE Trans. Dielectr. Electr. Insul., vol. 25, no. 4, pp. 1238-1247, Aug. 2018.
[11] N. Hayakawa *et al*, "Electric field grading by Functionally Graded Materials (FGM) for HVDC gas insulated power apparatus," *IEEE Conf. Electr. Insul. Dielect. Phenom. (CEIDP)*, 2018, 5-4, pp. 390-393.
[12] Rachmawati *et al*, "Electric field grading by permittivity and conductivity graded materials (ε/σ-FGM) for HVDC gas insulated power apparatus," *9th Int. Symp. Electr. Insul. Mat. (ISEIM)*, 2020, VF-6, pp. 421-424.
[13] U. Riechert *et al*, "Compact gas-insulated systems for high voltage direct current transmission: design and testing," *IEEE/PES Transmission and Distribution Conf. Expo. (T&D)*, 2016.
[14] U. Riechert, U. Straumann, and R. Gremaud, "Compact gas-insulated systems for high voltage direct current transmission: basic design," *IEEE/PES Transmission and Distribution Conf. Expo. (T&D)*, 2016.
[15] R. Nakane *et al*, "Electrical insulation performance of HVDC-GIS spacer under various testing conditions," *IEEE Conf. Electr. Insul. Dielect. Phenom. (CEIDP)*, 2017, 7-6, pp. 621-624.
[16] H. Li, N. Zebouchi, and A. Haddad, "Theoretical and practical investigations of spacer models for future HVDC GIL/GIS applications," *Proc. 21st Int. Symp. High Voltage Engineering (ISH)*, 2019, vol. 2, pp. 1538-1549.
[17] H. Koch *et al*, "High power underground transmission for HV DC", *CIGRE Session*, SC B3-104, Paris, 2016, pp. 1-11.
[18] Y. Miyazaki et al, "Breakdown characteristics of cone-type ε-FGM spacer for gas insulated switchgears," *9th Int. Symp. Electr. Insul. Mat. (ISEIM)*, 2020, VK-2, pp. 533-536.
[19] N. Hayakawa *et al*, "Development of cone-type FGM spacer for actual size GIS," *IEEE Conf. Electr. Insul. Dielect. Phenom. (CEIDP)*, 2020, 4A-3, pp. 269-272.

Rachmawati was born in Indonesia in 1988. She received the B.Sc. degree and M. Eng degree both in electrical engineering from Bandung Institute of Technology, Indonesia in 2010 and Tohoku University, Japan, in 2013, respectively. She is currently a doctoral student in Graduate School of Engineering, Nagoya University, Japan. She was an academic assistant in School of Engineering and Informatics (SEEI), Bandung Institute of Technology from 2017 to 2019. She is a student member of IEE of Japan and CIGRE.

Hiroki Kojima (M'11) was born in Japan, in 1975. He received his Ph.D degree in 2004 in energy engineering and science from Nagoya University. He was a Researcher Fellow with the Japan Society for the Promotion of Science from 2000 to 2003. Since 2004, he has been at Nagoya University and presently he is an Associate Professor of Nagoya University in the Department of Electrical Engineering. Dr. Kojima is a member of IEE of Japan.

Naoki Hayakawa (M'90) was born in Japan, in 1962. He received his Ph.D degree in 1991 in electrical engineering from Nagoya University. He has been at Nagoya University since 1990, where he is presently a Professor in the Department of Electrical Engineering. From 2001 to 2002, he was a guest scientist at the Forschungszentrum Karlsruhe, Germany. Prof. Hayakawa is a member of IEE of Japan and CIGRE.

Katsumi Kato was born in 1969. He received his Ph.D degree in 1997 in electrical engineering from Nagoya University. From 1997, he was on the faculty of Nagoya University. Currently he is an Associate Professor at the National Institute of Technology, Niihama College in the Department of Electrical Engineering and Information Science. Dr. Kato is a member of IEE of Japan.

Nabila Zebouchi received the PhD. degree in Electrical Engineering from the University Paul Sabatier, Toulouse, France, in 1997. She has worked at ABB AB Corporate Research in Sweden, at the French company Nexans manufacturer of high voltage cables and accessories and the Belgian Ceramic Research Centre. She participated as a full member from 2013 to 2019 to the CIGRE working group D1-56 dealing with Field Grading in Electrical Insulation Systems. She is presently working on FLEXIS Project-WP 16: Environmentally Friendly Electrical Power Plant and Insulation, at the Advanced High Voltage Engineering Research Centre, Cardiff University, UK.